

利用外來資訊轉換圖設計 位元交錯調變碼之迭代解碼系統

研究生：劉益彰

指導教授：沈文和 博士

國立交通大學

電信工程學系碩士班

摘要

外來資訊轉換圖是一個在迭代解碼系統中很好的分析解碼收斂行為的工具，在位元交錯調變碼的解碼系統中，位元對應的設計對於提升系統效能是非常重要的，藉由不同的平均位元差異數來改變訊號偵測器轉換曲線的斜率，因而從中選出一個最適合外部碼的位元對應方式。我們說明了這樣的作法的確可以大幅的改善系統效能。在這篇論文中，我們還提出了利用外來資訊轉換圖來設計柵欄移除(trellis-pruned)迴旋碼和穿刺(punctured)迴旋碼在位元交錯調變碼解碼系統中來達到不同的系統需求。

On the Design of the BICM-ID Systems with EXIT Chart

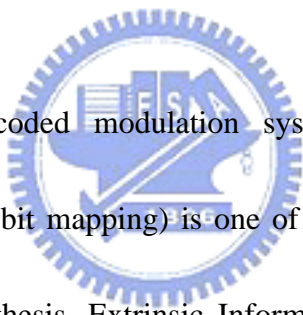
Student: Yi-Chang Liu

Advisor: Dr. Wern-Ho Sheen

Department of Communication Engineering

National Chiao Tung University

Abstract



In the bit-interleaved coded modulation systems with iterative decoding (BICM-ID), a good labeling (bit mapping) is one of the key factors that dictate the system performance. In this thesis, Extrinsic Information Transfer (EXIT) chart, a popular tool to analyze the convergence behavior of an iterative decoding system, is employed for the labeling design. By changing the slopes of the detector transfer curves and selecting the most suitable labeling for the outer code, we show that the system performance can be significantly improved. In addition, EXIT chart is employed to design good trellis-pruned and punctured convolutional codes in BICM-ID systems to provide different levels of performance and code rate trade off.

誌謝

這篇論文得以完成，主要是有指導教授 沈文和 博士的細心教導，在學術研究上沈文和老師一直是我的榜樣，不管是做研究的方法和態度都是我的學習對象，在研究過程中，常常是老師提供了許多建議，糾正了我很多錯誤的觀念，耐心的和我互相討論才能順利的寫出這篇論文。另外還要特別感謝王忠炫 博士，在我碩二時加入了實驗室的團隊，對於啟發我的想法功不可沒，幫助我在論文完成的路上更加的順暢。也要感謝口試委員 賴癸江 博士的一些建議，讓我的論文可以更加完善。

這二年的研究生活中，實驗室的同仁對我的幫助也很大，常常茶餘飯後和倉緯、昱帆和東融討論，許多的問題也是因為學長們的幫助才得以順利解決，正欣、志成、宜康等學長還有宸睿和相榮，特別要感謝畢業的鼎哲學長，給了我許多的建議，我的許多問題也是你不厭其煩的為我解答，謝謝你。平常生活中，有許多同學陪我一起玩、一起笑也一起苦，雄光、Q仔、阿龜、雄仔、死歐、慣風、中義…等，都是很要好的伙伴。

最後我要感謝我的家人，特別是我的爸媽，因為有你們才有現在的我，不管在生活上還是心理上一直都是我的最大的支柱，也從來不曾讓我失望過，所以我也不會讓你們失望，謝謝你們！

民國九十五年七月

研究生劉益彰謹識於交通大學

Contents

摘要	i
Abstract	ii
誌謝	iii
Contents	iv
List of Tables	vii
List of Figures	viii
Chapter 1 Introduction	1
Chapter 2 System Model	4
2.1 Encoder	6
2.2 Bit interleaving	6
2.3 Signal mapping	8
Chapter 3 Iterative Decoding of BICM Systems	11
3.1 APP detector	11
3.2 MAP decoder	12
Chapter 4 Extrinsic Information Transfer (EXIT) Charts	17
4.1 Transfer characteristics	18
4.2 Transfer curve simulations	21
4.2.1 Transfer characteristics of the detectors	21
4.2.2 Transfer characteristics of the decoders	24

4.2.3	EXIT chart	25
Chapter 5	Labeling design in BICM-ID systems	27
5.1	Labeling design	27
5.2	Simulation results	37
Chapter 6	Trellis-pruned and Punctured convolutional codes	38
6.1	Trellis-pruned convolutional codes	38
6.1.1	Encoding of the trellis-pruned convolutional codes	38
6.1.2	Decoding of the trellis-pruned convolutional codes	39
6.1.3	Decoder transfer characteristics with trellis pruning	41
6.1.4	Performance	43
6.2	Punctured convolutional codes	45
6.2.1	Minimum free distance	46
6.2.1.1	Puncturing design on rate 2/3 codes	47
6.2.1.2	Puncturing design on rate 3/4 codes	49
6.2.2	Puncturing patterns design with EXIT chart	51
6.2.2.1	Rate 2/3 codes	52
6.2.2.1.1	(5 ₈ ,8 ₈) convolutional codes	52
6.2.2.1.2	(133 ₈ ,171 ₈) convolutional codes	53
6.2.2.2	Rate 3/4 codes	54
6.2.2.2.1	(5 ₈ ,8 ₈) convolutional codes	54

6.2.2.2.2 $(133_8, 171_8)$ convolutional codes	56
6.2.3 Summary on puncturing design	58
Chapter 7 Conclusions and future works	59
7.1 Conclusions	59
7.2 Future works	60
References	61



List of Tables

Table 6-1: The number of incorrect paths for the rate-2/3 punctured $(5_8, 7_8)$ and $(133_8, 171_8)$ codes	48
Table 6-2: The total number of the error bits produced by the incorrect paths for the rate-2/3 punctured $(5_8, 7_8)$ and $(133_8, 171_8)$ codes	48
Table 6-3: The number of incorrect paths for the rate-3/4 punctured $(5_8, 7_8)$ and $(133_8, 171_8)$ codes	50
Table 6-4: The total number of the error bits produced by the incorrect paths for the rate-3/4 punctured $(5_8, 7_8)$ and $(133_8, 171_8)$ codes	51



List of Figures

Fig. 2-1: Transmitter	4
Fig. 2-2: Receiver	4
Fig. 2-3: The convolutional encoder (K=7, R=1/2)	6
Fig. 2-4: 16QAM, Anti-Gray labeling	8
Fig. 2-5: 16QAM, Gray labeling	9
Fig. 2-6: 64QAM, Gray labeling	9
Fig. 2-7: 16QAM, Natural labeling	10
Fig. 2-8: 64QAM, Natural labeling	10
Fig. 4-1: Receiver diagram of a serial concatenated system	17
Fig. 4-2: Extrinsic information transfer characteristics of the inner detector for Natural, AntiGray and Gray mapping at $E_b / N_0 = 3dB$ with 16QAM and single antenna.	22
Fig. 4-3: Extrinsic information transfer characteristics of the inner detector for 16QAM, Natural mapping at $E_b / N_0 = 1dB, 3dB, 5dB$ and $7dB$.	22
Fig. 4-4: Extrinsic information transfer characteristics of the inner detector for 16QAM, Gray mapping at $E_b / N_0 = 1dB, 3dB, 5dB$ and $7dB$	23
Fig. 4-5: Extrinsic information transfer characteristics of the inner detector for 16QAM ,Anti-Gray mapping at $E_b / N_0 = 1dB, 3dB, 5dB$ and $7dB$	23
Fig. 4-6: Extrinsic information transfer characteristics of the outer decoder for different generator polynomial with code rate 1/2.	24
Fig. 4-7: Extrinsic information transfer characteristics of the outer decoder for the $(133_8, 171_8)$ convolutional code with different punctured code rate.	25
Fig. 4-8: EXIT chart of a serial concatenated system with APP detector and a $(133_8, 171_8)$ convolutional code, 16QAM and Anti-Gray mapping.	26
Fig. 5-1: Subset partitions of 16QAM for Natural constellations.	29
Fig. 5-2: Subset partitions of 16QAM for Type A constellations.	30
Fig. 5-3: Subset partitions of 16QAM for Type B constellations.	31
Fig. 5-4: Subset partitions of 16QAM for Type C constellations.	32
Fig. 5-5: Detector transfer characteristics for six mappings at $E_b / N_0 = 3dB$ and 16-QAM.	34
Fig. 5-6: EXIT chart for six mappings at $E_b / N_0 = 3.5 dB$ and 16-QAM.	34
Fig. 5-7: Type A mapping for 64QAM.	35
Fig. 5-8: Type B mapping for 64QAM.	36

Fig. 5-9: Type C mapping for 64QAM.	36
Fig. 5-10: BER of BICM-ID with six mappings with the $(133_8, 171_8)$ convolutional code, 16QAM , 20 iterations.	37
Fig. 6-1: Trellis-pruned convolutional encoder	38
Fig. 6-2: Decoding trellis (a) the original convolutional codes (b) the trellis-pruned convolutional code	40
Fig. 6-3: Transfer characteristics of the decoder with $K=3,4,6,30$ and the original code, the generator polynomial is $(g_0, g_1) = (133_8, 171_8)$.	41
Fig. 6-4: The zoom in vision of Fig.6-3.	42
Fig. 6-5: EXIT chart for different bit-mappings in 16QAM BICM-ID systems at $E_b / N_0 = 2dB$.	43
Fig. 6-6: BER of BICM-ID with six mappings with the $K=4$ trellis-pruned $(133_8, 171_8)$ convolutional code, 16QAM , 20 iterations.	44
Fig. 6-7: BER of the BICM-ID systems with trellis-pruned and original convolutional codes, 16QAM, 20 iterations, both are Type B labeling.	44
Fig. 6-8: EXIT chart of the punctured codes with puncturing matrices \mathbf{P}_1 and \mathbf{P}_2 at $E_b / N_0 = 7dB$ with 16QAM AntiGray mapping and generator polynomial $(g_0, g_1) = (5_8, 7_8)$.	53
Fig. 6-9: EXIT chart of the punctured codes with puncturing matrices \mathbf{P}_1 and \mathbf{P}_2 at $E_b / N_0 = 5dB$ with 16QAM AntiGray mapping and generator polynomial $(g_0, g_1) = (133_8, 171_8)$.	54
Fig. 6-10: EXIT chart of the punctured codes with puncturing matrices \mathbf{P}_1 to \mathbf{P}_5 at $E_b / N_0 = 8dB$ with 16QAM Natural mapping and generator polynomial $(g_0, g_1) = (5_8, 7_8)$.	55
Fig. 6-11: The same chart as Fig.5-3, but the range is from about 0.9 to 1.	56
Fig. 6-12: EXIT chart of the punctured codes with puncturing matrices \mathbf{P}_1 to \mathbf{P}_5 at $E_b / N_0 = 7dB$ with 16QAM Natural mapping and generator polynomial $(g_0, g_1) = (133_8, 171_8)$.	57
Fig. 6-13: The same chart as Fig.5-5, but the range is from about 0.9 to 1.	57